Characterization of the α-relaxation and gel-like dynamics in mixed network forming $(GeO_2)_x(NaPO_3)_{100-x}$ glass melts by photon correlation spectroscopy

David L. Sidebottom
Creighton University

Abstract

Dynamic light scattering investigations of the α-relaxation in network-forming $(GeO_2)_x(NaPO_3)_{100-x}$ glass melts is reported for x = 0 to 40 mol% GeO_2. Addition of GeO_2 results in an increased density of bridging oxygen bonds. This monotonically increases the glass transition temperature but generates complex changes to the glass forming fragility which initially decreases with increasing GeO_2 but increases again at higher GeO_2 contents. A resolution to this odd fragility behavior is obtained by applying a coarse-graining procedure used previously in sodium germanate melts to arrive at a topological network connectivity for which fragility exhibits a universal dependence. Also observed in the light scattering measurements is a secondary relaxation, several orders of magnitude slower than that of the α-relaxation, which we tentatively attribute to gel-like anomalous diffusion of Ge crosslinks formed between phosphate chains.

I. Introduction

Near the glass transition, supercooled liquids display viscous relaxation that is characteristically non-exponential and which evolves with a timescale whose temperature dependence is non-Arrhenius [1,2]. These non-canonical dynamics are believed to stem from the complexity of molecular rearrangements [2] needed for viscous flow as a liquid approaches the glass transition temperature - a temperature (T_g) where the viscosity reaches $\eta \sim 10^{12}$ Pas and rearrangements require $\langle \tau_\alpha \rangle \sim$ 100s of seconds [1]. The non-exponential relaxation is commonly described by a stretched exponential of the form,

$$exp\{-(t/\tau)^\beta\}, \quad (1)$$

where the stretching exponent, β, is either a measure of the distribution of relaxation times (if the relaxation arises from dynamically heterogeneous regions [3]) or a measure of the coupling or cooperativity of the rearrangement process (if the relaxation occurs homogeneously [4]). The non-Arrhenius temperature dependence is commonly characterized by the kinetic fragility [1],

$$m = \left.\frac{d\log_{10}\langle\tau_\alpha\rangle}{d(T_g/T)}\right|_{T\to T_g}, \quad (2)$$

which is a measure of the rapidness with which a glass regains liquid-like flow on heating above T_g. The fragility is also associated with the rate at which configurational entropy [5,6], lost in the transition to a non-ergodic state, is reclaimed when heated above T_g. Fragile liquids ($m \geq 60$) are represented by a large population of molecular liquids and organic polymers for which van der Waals forces provide cohesion. Strong liquids ($16 < m < 30$) are mainly represented by a handful of network-forming oxides (NFOs) like SiO_2 ($m = 20$) which form continuous random networks of covalently bonded atoms and feature in most commercial and technical applications of glass.

Despite the commercial significance of NFOs, studies of glass-forming dynamics in supercooled liquids over the last half century have been heavily weighted toward investigations on simple molecular and ionic liquids, many conducted using broadband dielectric spectroscopy which conveniently probes viscous relaxation via dipolar reorientations [7]. Consequently, theories for liquids [8] and glass-forming liquids [9] describe only hard-sphere-like models with isotropic, Lennard-Jones-like potentials designed to apply specifically to these simple liquids. Covalently bonded NFOs are often dismissed as being too complex owing to their discrete and directional bonding.

However, because the NFOs form discrete and highly directional bonds between the constituent atoms, their bond structure can often be quantified by spectroscopies like nuclear magnetic resonance (NMR). This structural information has contributed to recent approaches which seek to model compositional trends in glass properties like hardness, T_g and fragility through an analysis of the mechanical constraints introduced by the covalent bonds [10-13].

Key to modeling is the interplay between the mechanical constraints and the degrees of freedom of the atoms [10]. In the mean field version of this approach [11], a critical atomic bond density, $\langle r \rangle$ = 2.4 bonds per atom is highlighted where on average there are just sufficient constraints to offset all the atomic degrees of freedom. Networks below this rigidity percolation threshold are under-constrained and "floppy" while those above are over-constrained and rigid [11]. It is presumed that these extremes of network connectivity in the solid should also influence dynamics in the supercooled liquid. Viscous flow in NFOs often involves the temporary rupture of local bridging oxygen (BO) bonds. In over-constrained networks, the development of fluidity would be suppressed by the need to rupture multiple bridging bonds leading to a low fragility and high T_g. By contrast, an under-constrained network that requires far few bond-breaking events to become fluid should have a lower T_g and presumably be more fragile.

Our recent efforts [6,14-18] have focused on dynamic light scattering measurements of the primary α-relaxation in certain NFOs for which the bond structure has been well characterized by NMR or other spectroscopies. The goal is to address a data gap in the glass transition literature in which far more studies of this relaxation in molecular liquids (primarily using dielectric spectroscopy) exist than do comparable studies of NFOs (whose dynamics require temperatures well above ambient where dielectric spectroscopy becomes challenging). Moreover, because NFOs can be altered by chemical means to achieve continuous changes in the network connectivity ranging from polymeric chains to continuous random networks, they offer an important avenue for exploring the role of glass structure for the non-Arrhenius and non-exponential character of dynamics in the melt. An important outcome of our investigations has been the realization that the fragility in network-forming glasses exhibits a *universal* dependence on the topological connectivity of the network. This has been illustrated [6] for more than 150 different network-forming glasses but does require special treatment (discussed later) of certain mesoscopic structural units whose proper connectivity must be determined by a well-defined coarse-graining procedure [19].

In the present study, we investigate the *mixed network* forming system $(GeO_2)_x(NaPO_3)_{100-x}$ for which a recent NMR investigation[20] has provided the quantities of 2, 3,

and 4-coordinate species present in the network for compositions from x = 0 to 50 mol% GeO_2. $NaPO_3$ is comprised of polymeric chains [21] of PO_4 tetrahedra which become crosslinked by the addition of GeO_2 resulting in increased bond density. Here we augment this structural picture with new dynamic light scattering measurements of the viscous dynamics as conveyed by the primary α-relaxation appearing in the dynamic structure factor [22,23]. In addition to characterizing the fragility of these melts and the non-exponentiality of the relaxation, we also observe a secondary relaxation process at longer relaxation times that we attribute to a gel-like anomalous diffusion of Ge crosslinks. In analyzing the fragility, we again apply coarse-graining to properly assess the topological connectivity of the oxide network.

II. Experimental

A. Sample Preparation

A stock of $NaPO_3$ was prepared by reacting ammonium dihydrogen phosphate ($NH_4H_2PO_4$, 99.999%) with Na_2CO_3 (99.95%, dissolved, filtered at 0.22 μm and dehydrated prior to use in an effort to eliminate insoluble particulates) at approximately 330 C until the weight matched the batch expectation. This was then mixed with GeO_2 (99.9999%) in appropriate amounts and dried at 400 C in a silica crucible for one-half hour before being melted at temperatures between 950 and 1000 C for one hour. Each melt was poured to form several slender ingots (approximately 4 mm dia. by 3 cm in length) that were stored in a desiccator for later use. For photon correlation spectroscopy (PCS) studies, one or more ingots were loaded into a pre-cleaned silica ampoule (6 mm ID x 8 mm OD) that served as the light scattering cell. The contents of the ampoule were remelted and degassed before being transferred to a pre-heated optical furnace.

B. Light Scattering

Vertically polarized laser light (532 nm) was focused to approximately 50 μm beam waist in the sample and the light scattered at θ = 90 degrees was passed through a laser line filter (to reduce unwanted radiation from the optical furnace) before being imaged by a lens onto a 50 μm pinhole located approximately 40 cm from the photosensitive surface of a photomultiplier

tube (PMT). The diffraction of the light by the pinhole influences the signal-to-noise for detecting intensity fluctuations, $I(t')$, and the corresponding coherence factor [22], A_{COH} = 0.80, was calibrated separately. Photopulses from the PMT were amplified and digitized before arriving a commercial correlator which calculated the time-averaged intensity-intensity autocorrelation function,

$$C(t) = \frac{\langle I(t\prime)I(t\prime+t)\rangle}{\langle I(t\prime)\rangle^2} = 1 + A_{COH}|S(q,t)|^2, \quad (3)$$

where $S(q,t)$ is the dynamic structure factor [22,23]. Autocorrelation functions were collected at a series of fixed temperatures as each sample was cooled on approach to the glass transition. Spectra were later fit by appropriate decay functions described momentarily.

III. Results

For compositions of $(GeO_2)_x(NaPO_3)_{100-x}$ with x = 0 to 30%, clear, transparent and stable liquids were obtained that could be studied over wide temperature ranges. Samples at 35 and 40%, however, became progressively less stable to phase separation and data for the 40% sample could only be obtained by quenching to temperatures below 570 C. Samples produced at 45 and 50% exhibited partly opaque appearance when cast into ingots and were deemed too unstable to study in the liquid phase. This is consistent with reports by the NMR researchers [20] who could not obtain transparent glasses at x > 50 mol% GeO_2.

The sodium metaphosphate (x = 0) melt has been previously examined [14] and exhibits only a single, non-exponential relaxation that is independent of the scattering angle (hence independent of the scattering wavevector [22,23], $q = 4\pi n \sin(\theta/2)/\lambda$). The non-exponentiality of this decay along with its q-independence and its approach to a relaxation time of 100 seconds near T_g establish it to be the primary α-relaxation [23]. However, for all compositions in which GeO_2 is added, a second relaxation process is observed at long times in addition to the α-relaxation seen at shorter times as shown in Fig. 1. A separate study of the angle dependence in the x = 20 mol% sample, reveals that the relaxation time for this second decay, τ_S, is approximately q^{-2}- dependent (see insert to Fig. 1) which identifies this as a

diffusive process likely associated with concentration fluctuations present in these GeO_2-containing melts. Although there is some indication that at x ≥ 30% this secondary relaxation could be better fit as two exponential decays with relaxation times less than two decades apart, we have opted to fit both the fast decay and the slow decay as separated stretched exponentials:

$$C_F(t) = 1 + B + A_{COH}\left|A_F exp\left[-(t/\tau_F)^{\beta_F}\right]\right|^2, \quad (4)$$

$$C_S(t) = 1 + A_{COH}\left|A_S exp\left[-(t/\tau_S)^{\beta_S}\right]\right|^2. \quad (5)$$

Results for the stretching exponents, β_F and β_S, are shown in Fig. 2. The non-exponentiality of the α-relaxation is found to be largely independent of the addition of GeO_2 while that of the slow relaxation initially decreases with increasing GeO_2 and remains constant near β_S = 0.6 at concentrations above 20 mol%.

Results for the relaxation times, τ_F and τ_S, of the fast and slow relaxations are presented as a function of temperature in Figs. 3 and 4, respectively. Due to inherent limitations of the correlator time window (approximately 100 ns to 100s of seconds) along with practical limits on the time needed to accumulate an adequate time average for ultra-slow decay processes, the slow relaxation is mainly observed at higher temperatures before it eventually passes beyond the time window as T_g is approached. As seen in Fig. 4, the slow relaxation time exhibits a pronounced curvature with temperature appearing to approach a constant value in the limit of ultra-high temperatures. By contrast, the fast α-relaxation that is visible mainly at lower temperatures exhibits relaxation times with far less curvature and which approach values of 100 seconds near the T_g reported in the literature [20].

As is customary [23], the average α-relaxation time,

$$\langle\tau_\alpha\rangle = \int_0^\infty exp\{-(t/\tau_F)^{\beta_F}\}dt = \frac{\Gamma(1/\beta_F)\tau_F}{\beta_F}, \quad (6)$$

has been extrapolated to 100 seconds to experimentally determine the glass transition temperatures of the samples. These are presented in Fig. 5 along with the literature values

obtained by differential scanning calorimetry and, with a one possible exception, show good agreement between the two studies given that T_g is being determined by different methods. With the glass transition temperature so determined, a plot of $\log_{10}\langle\tau_\alpha\rangle$ against T_g/T can then be constructed from which the fragility index m can be assessed (see Eqn. 2) as the slope near T_g. Results for the fragility are also included in Fig. 5 and show a rapid factor of two decrease in m with initial addition of GeO_2 up to x = 15 mol% followed by an increase to values near m = 60 for glasses with x $\geq$ 30 mol%. These and other results are summarized in Table 1.

IV. Discussion

A. The Slow Relaxation

In previous light scattering studies of both sodium borate [16] and sodium germanate [17] glass melts a secondary relaxation was encountered at times longer than the α-relaxation provided the sodium oxide content was non-zero but less than about 10 mol% Na_2O. There the slow relaxation was also diffusive but exponential (β_S = 1) and was associated with concentration fluctuations arising from the diffusion of mobile sodium ions within the oxide network. The disappearance of this secondary relaxation at ion concentrations above 10 mol% Na_2O is thought to be caused by a dwindling signal-to-noise for detecting these fluctuations as the scattering sources become too concentrated [16].

The secondary relaxation found in the present case, however, is not of the same origin as that observed previously. For one thing, the sodium oxide content of all the samples in the present study remains well above the 10 mol% Na_2O threshold for which the ionic relaxation should no longer be detectable. Furthermore, the relaxation found here is clearly non-exponential. Given that this secondary relaxation only appears with the addition of GeO_2, we suggest an alternative source for the dynamical feature. $NaPO_3$ has a polymeric structure [21] consisting of chains of PO_4 tetrahedra linked together by two BO bonds in which the sodium ions reside in interstitial locations weakly bonded to the two terminal oxygens of the tetrahedron and yet remain mobile with respect to the oxide network. As GeO_2 is added, it enters into the oxide network as either 3-coordinated (Ge^3) or 4-coordinated (Ge^4) units [20] that crosslink together three or four phosphate chains, respectively. Initially, these Ge atoms

are well separated and because the Ge atom has roughly twice the polarizability of the surrounding P atoms the Ge crosslinks elastically scatter light with greater intensity. The relative motions of the diffusing Ge crosslinks would then give rise to additional intensity fluctuations detected by the PMT resulting in a secondary decay in the autocorrelation function much like what we observe.

To the extent for which the diffusion of these Ge scatters can be regarded as the result of Brownian-like motion, the diffusivity should then, particularly at low GeO_2 contents, be largely determined by the viscosity of the surrounding metaphosphate melt. Thus, over a range of temperatures, τ_S should remain proportional to that of the α-relaxation time. Unfortunately, this notion could not be effectively tested. Due to the large separation in time between the two relaxations ($\tau_S/\tau_\alpha \sim 10^5$) compounded by the limited window of the correlator, simultaneous values of τ_S and τ_α were available only for very narrow temperature ranges. Instead, support is presented in Fig. 6 where both the α-relaxation time and the slow relaxation time have been super-imposed by effectively dividing τ_S by 2 x 10^5. Here, the alignment of the shifted slow relaxation time with the fast α-relaxation time gives the appearance of a continuous temperature variation that increases slowly with cooling at high temperatures but increases more rapidly nearer to T_g. The α-relaxation time is known to be proportional [23] to the melt viscosity with $\langle\tau_\alpha\rangle \approx 10^{-10}\,\eta$ (in Pas) near T_g and the continuous temperature variation in Fig. 6 is remarkably similar with that of the viscosity found in other oxide melts, like B_2O_3 [24] (see inset to Fig. 6).

It is important to emphasize that the shift of the slow relaxation time by 2 x 10^5 in Fig. 6 is not entirely arbitrary. As a self-similar process, diffusion is characterized by a probability distribution with a Gaussian profile,

$$G(r,t) = \frac{1}{\sqrt{6\pi Dt}} e^{-r^2/6Dt}, \qquad (7)$$

that decreases in amplitude and spreads out as the mean squared displacement (MSD) of diffusing particles, $\Delta r^2 = 6Dt$, increases in time. The spatial Fourier transform of this is an exponential decay of the form,

$$S(q,t) = S(q,0)e^{-q^2Dt}, \quad (8)$$

with relaxation time that scales with q^{-2} as $\tau_S = 1/Dq^2$, where D is the diffusivity [22]. This is the diffusive feature we observe as a slow relaxation in our PCS measurements. However, our particular $\tau_S(T)$ seen for light scattering at $\theta = 90°$ is not *inherently special*. In fact, as shown in the inset of Fig. 1, measurements at other scattering angles would produce a different $\tau_S(T)$. Physically, this q-dependence amounts to how different scattering studies can sample the same, self-similar Gaussian distribution (Eq. 7) at differing length scales. For our light scattering with q = 25 μm^{-1}, the prominent intensity fluctuations correspond to phase changes in the scattered electric field of $e^{-i\vec{q}\cdot\overrightarrow{\Delta r}}$ where $\Delta r \sim 2\pi/q$ and amount to relative displacements of Ge atoms by distances of Δr nearly half the wavelength of our light source. Such large MSDs require corresponding long relaxation times. Thus, the shift of 2 x 10^5 applied to our τ_S really amounts to an examination of the diffusion *as it would appear* over a shorter Δr.

But is there some inherently special timescale for diffusion? Consider the random walk model in which the Ge scatterer makes discrete steps of some distance R_o in random directions to be repeated on a time interval t_o. These discrete steps are intended to model the random perturbations from the surrounding medium (here, the segmental motions of polymeric PO_4 chains happening on the viscoelastic timescale of the α-relaxation). Given the q^{-2} dependence, we find that the shift by 2 x 10^5 corresponds to scattering at q = 1.12 $Å^{-1}$ and displacements of only $\Delta r \approx 5$ Å - a distance comparable to the diameter of a GeO_4 unit and appropriate for the stepping distance (R_o) of a random walker! We conclude that the slow relaxation has its microscopic origins in that of the fast relaxation and both share a common dependence on the viscosity of the melt itself.

But why is the slow relaxation non-exponential? We believe this non-exponentiality is a consequence of how the Ge atoms are partially constrained in their motions by virtue of their incorporation into the phosphate chains as crosslinks. In principle, each Ge atom is attached by a phosphate chain to a neighboring Ge atom and the length of the intervening chain places a limit on the relative displacement of the two scatterers. Moreover, each Ge joins three or four

chains together and this results in additional constraints to the diffusion of the Ge atoms. A restriction of the available space for Ge diffusion occurs and becomes more severe when the average interconnecting chain length shortens as the population of Ge crosslinks increases. An estimate of the average number of PO_4 units within a chain connecting two Ge atoms is given roughly as half the P:Ge ratio (see Fig. 2) and would diminish to less than 2 at concentrations above 25 mol% GeO_2 which, interestingly, is where β_S ceases to decrease and becomes fixed. Constrained diffusion such as this is often modeled by a random walk confined to a fractal space and is frequently manifested in the dynamics of gels near the sol-to-gel transition [25-27]. This "anomalous" diffusion results in MSD $\sim t^{\beta}$ with a corresponding stretched exponential decay of the structure factor much like we observe for the slow relaxation. Indeed, the decrease in β_S with the initial addition of GeO_2 crosslinks (see Fig. 2) is nearly identical to the decrease of β reported for structural relaxation in cluster-forming polyurethane gels [26] as the gel concentration increased and likewise consistent with the decrease in β in physical gels [27] as the gel temperature is approached.

B. The Fragility

As alluded to in the introduction, our previous investigations concluded that fragility in NFOs exhibits a universal dependence on topological connectivity of the oxide network. Initial support for this came from a study [14] of sodium phosphate glass melts in which we serendipitously chose to plot the fragility index as a function of the average BO bond density per P atom, $\langle n \rangle$, as is shown in Fig. 7, essentially treating the oxide network as a collection of PO_4 tetrahedra linked by BO connections. As sodium is removed the BO bond density increases and we observed the fragility index initially decrease with $\langle n \rangle$, plateau slightly below $\langle n \rangle$ = 2.4 and then decrease to m = 19 for P_2O_5 with $\langle n \rangle$ = 3. At that time, we remarked on the coincidence of this fragility-versus-connectivity pattern to that which results when the fragility of $As_xGe_xSe_{100-2x}$ [28,29] is plotted as a function of the average *atomic* bond density, $\langle r \rangle$ as is included in Fig. 7. This coincidence suggested that a type of *coarse-graining* [19] of the network connectivity is required for the fragility: whereas the average atomic bond density is the relevant metric of network connectivity for the oxide-free chalcogenides, the rigid nature of the

PO_4 tetrahedra in the oxide glass allows it to resist internal deformations during viscous flow causing the BO connections between tetrahedra to become the relevant metric of topological connectivity.

In the present case, we can determine the average BO bond density of the $(GeO_2)_x(NaPO_3)_{100-x}$ glasses using results from the nuclear magnetic resonance (NMR) study by Ren and Eckert [20]. Their investigation reported phosphate units P^1, P^2 and P^3 and germanate units Ge^3 and Ge^4, where each superscript indicates the BO per atom, and quantified the fractions $f_{P1}(x)$, $f_{P2}(x)$, $f_{P3}(x)$, $f_{Ge3}(x)$ and $f_{Ge4}(x)$, respectively, as a function of the concentration of GeO_2 added. The values are reproduced here in Fig. 8. Using this data, the average BO bond density can be determined as

$$\langle n \rangle = 0 \times f_{P1} + 2 \times f_{P2} + 3 \times (f_{P3} + f_{Ge3}) + 4 \times f_{Ge4}, \quad (9)$$

where a P^1 unit operates as a dangling unit with zero topological connectivity [11]. In Fig. 7 we have replotted the fragility of the $(GeO_2)_x(NaPO_3)_{100-x}$ glass melts now as a function of the average BO bond density. In this plot, $m(\langle n \rangle)$ coincides well with the mastercurve (dashed line) for x $\leq$ 10 mol% GeO_2 but noticeable deviations appear at higher GeO_2 concentrations.

Deviations of this sort have been encountered before. In previous investigations of the fragility of both sodium borate [30] and sodium germanate [31] glasses substantial deviations of $m(\langle n \rangle)$ from the mastercurve were encountered including *increases* of m with increasing $\langle n \rangle$ that sharply contradict the trends in the chalcogenide and sodium phosphate cases. To attempt a resolution to this contradiction for the sodium borates, we contemplated the role of small boroxol rings that are found abundantly (about $f_R = 70\%$ of B are participants in rings) in B_2O_3. We speculated that, much like the rigid PO_4 tetrahedron in alkali phosphates, these rings function as a larger rigid structural unit and that a coarse-graining adjustment was required to ascertain the proper topological connectivity of those boron units participating in rings. It was reasoned that although a borate unit would normally have n = 3 BO connections, a unit participating in a ring would have only ϕ = 2 topological connections owing to the redundancy of one of the two BOs that attach the unit to the ring. Applying this strategy for B_2O_3 led to a

coarse-grained connectivity of $\phi = 2 \times f_R + 3 \times (1 - f_R) \approx 2 \times (0.7) + 3 \times (0.3) = 2.3$, far smaller than $\langle n \rangle$ = 3, but which is found to position $m(\phi) \sim 32$ onto the mastercurve in Fig. 7. When this coarse-graining was applied to the rings and other small rigid units over an extended range of added sodium oxide [30], the increasing $m(\langle n \rangle)$ was converted to a decreasing $m(\phi)$ that coincided perfectly with the mastercurve in Fig. 7.

In the instance of sodium germanates, a similar coarse-graining was applied [31]. There, evidence for the existence of small, 3-membered rings was provided by Raman spectroscopy. Henderson[32] has argued that the Raman mode in the vicinity of 520 cm^{-1} is to be associated with small rings, similar to the boroxol ring but comprised of 4 or 5-coordinated germanate units depending on the alkali content. In $(Na_2O)_x(GeO_2)_{100-x}$, this Raman mode increased rapidly from x = 0 to x = 10 mol% and saturated in intensity by x = 20 mol%. In the coarse-graining approach, we modeled the increase by a ring fraction, $f_R(x)$ that began at 45% in GeO_2 and increased to about 80% for x = 20 mol% Na_2O. Assuming a random distribution of Ge^4 and Ge^5 units in rings along with known fractions $f_{Ge4}(x)$ and $f_{Ge5}(x)$ based on stoichiometry, the coarse-grained connectivity was estimated as

$$\phi = f_{NR}(4 \times f_{Ge4} + 5 \times f_{Ge5}) + f_R f_{NR}(3 \times f_{Ge4} + 4 \times f_{Ge5}) + f_R^2(0 \times f_{Ge4} + 2 \times f_{Ge5}), \quad (10)$$

where $f_{NR}(x) = 1 - f_R(x)$. The middle term refers to units participating only in a single ring and the last term refers to units that are simultaneously participating in two rings. In this last case, the Ge^4 unit is considered to have zero topological connectivity as it is internal to the double ring which itself comprises a rigid structural unit (see inset to Fig. 9).

To apply coarse-graining to the present $(GeO_2)_x(NaPO_3)_{100-x}$ system, we proceed in an *identical* manner. In the paper by Ren and Eckert [20], Raman spectra were provided for glasses with x = 0 to 50 mol%. As presented in their paper, these Raman spectra were normalized by the largest feature which for glasses below 30 mol% GeO_2 is the mode near 1150 cm^{-1} that is associated with the PO_2 symmetric stretching vibration but above 30 mol% is the ring mode itself near 520 cm^{-1}. Clearly the ring mode is increasing with added GeO_2 in the region up to x =

30 mol% and the fraction of rings can be roughly estimated by the Raman intensity at 520 cm^{-1}, $I_{520}(x)$, as $f_R(x) \approx I_{520}(x)/I_o$ where I_o is an unknown constant to be determined by curve fitting to be described shortly.

Because every fragility value shown in Fig. 7 for $(GeO_2)_x(NaPO_3)_{100-x}$ is larger than m = 40, there is only one possible value of ϕ residing on the mastercurve and so for each fragility a required connectivity, ϕ_{req}, can be defined. The value of I_o was then adjusted so that the difference between ϕ_{req} and the coarse-grained connectivity given by

$$\phi = f_{NR}(0 \times f_{P1} + 2 \times f_{P2} + 3 \times (f_{P3} + f_{Ge3}) + 4 \times f_{Ge4}) \\ + f_R f_{NR}(0 \times f_{P2} + 2 \times (f_{P3} + f_{Ge3}) + 3 \times f_{Ge4}) + f_R^2(0 \times f_{Ge4}), \qquad (11)$$

is minimized for samples from x = 0 to x = 30 mol%. It should be stressed here that I_o is the *only adjustable parameter* in the minimization as all the fractions of structural units come directly from Fig. 8. The resulting compositional variation of the ring fraction so obtained is plotted in Fig. 9 along with value of $f_R(x = 100)$ = 45% that was used for GeO_2 in previous coarse-graining of sodium germanates discussed above and reflects the self-consistency of our approach. In addition to values of $f_R(x)$ determined directly from the intensity of the Raman mode, values for x = 35 and 40 % have been estimated by extrapolation. Finally, when the fragility is replotted in Fig. 7 as $m(\phi)$ an excellent collapse of all values to the mastercurve in the region between ϕ = 2 to 2.2 is observed.

V. Conclusions

Glass forming dynamics in covalently-bonded network-forming liquids have received far less attention than have their isotropically-bonded simple liquid counterparts even though both have non-Arrhenius and non-exponential relaxation in common. In this regard, our present dynamic light scattering study of network-forming germano-phosphate glass melts provides much needed new insight into the viscous dynamics of these under-examined supercooled liquids and highlights the important significance of topological network connectivity in determining the fragility. Here, additional evidence for a universal dependence of fragility on

network connectivity [19] is found provided the topological connectivity of certain small ring structures is appropriately treated using the coarse-graining procedures adopted previously. An unexpected feature of the dynamic structure factor measured in the present germano-phosphate melts is a secondary relaxation process occurring far slower than the primary α-relaxation. This additional mode exhibits a non-exponential decay similar to that seen in sol-gel materials and we currently attribute it to the anomalous diffusion of Ge crosslinks constrained by phosphate chains.

Acknowledgement: This material is based upon work supported by the National Science Foundation under Grant No. (DMR-2051396)

References

1. P. G. Debenedetti and F. H. Stillinger, Supercooled liquids and the glass transition, Nature **410,** 259 - 267 (2001).
2. M. D. Ediger, C. A. Angell, and S. R. Nagel, Supercooled liquids and glasses, J. Phys. Chem. **100,** 13200-13212 (1996).
5. M. D. Ediger, Spatially Heterogeneous Dynamics in Supercooled Liquids, Annu. Rev. Phys. Chem. **51**, 99 - 128 (2000).
4. R. Richert, Homogeneous dispersion of dielectric responses in a simple glass, J. Non-Cryst. Sol. **172**, 209-213 (1994).
5. L-M. Martinez and C. A. Angell, A thermodynamic connection to the fragility of glass-forming liquids, Nature **410**, 663-667 (2001).
6. D.L. Sidebottom, Fragility of network-forming glasses: A universal dependence on the topological connectivity, Phys. Rev. E **92**, 062804 (2015).
7. R. Richert, Supercooled liquids and glasses by dielectric relaxation spectroscopy, Adv. Chem. Phys. **156**, 101-195 (2014).
8. J. P. Hansen and I. R. McDonald, *Theory of Simple Liquids* (Academic Press, London, 1986).
9. W. Goetze, *Complex Dynamics of Glass-forming Liquids: A Mode-Coupling Theory* (Oxford University Press, Oxford, 2009).

10. J.C. Phillips, Topology of covalent non-crystalline solids I: Short-range order in chalcogenide alloys. J. Non-Cryst. Sol. **34**(2): 153-181 (1979).
11. H. He and M. F. Thorpe, Elastic properties of glasses. Phys. Rev. Lett. **54**(19): 2107-2110 (1985).
12. J. C. Mauro, P. K. Gupta, and R. J. Loucks, Composition dependence of glass transition temperature and fragility II: A topological model of alkali borate liquids, J. Chem. Phys. **130** 234503 (2009).
13. M. M. Smedskjaer, J. C. Mauro, and Y. Yue, Prediction of glass hardness using temperature-dependent constraint theory, Phys. Rev. Lett. ***105***(11), 115503 (2010).
14. R. Fabian, Jr. and D.L. Sidebottom, Dynamic light scattering in network-forming sodium ultra-phosphate liquids near the glass transition, Phys. Rev. B **80**, 064201 (2009).
15. H. Uppala and D. L. Sidebottom, Evidence for ionic diffusion in dynamic light scattering from glass-forming sodium borate melts, J. Non-Cryst. Sol. **588***,* 121627 (2022).
16. D. L. Sidebottom, Dynamic light scattering study of the non-exponential α-relaxation in sodium germanate glass melts, J. Non-Cryst. Sol. (submitted Nov. 2023).
17. T. D. Tran and D. L. Sidebottom, Glass-forming Dynamics of Aluminophosphate Melts Studied by Photon Correlation Spectroscopy, J. Am. Ceram. Soc. **96**, 2147 (2013).
18. D. L. Sidebottom, Generic α-relaxation in a strong GeO_2 glass melt, Phys. Rev. E **107**, L012602 (2023).
19. D. L. Sidebottom, Connecting glass-forming fragility to network topology, Front. Mat. **6,** 114 (2019).
20. J. Ren and H. Eckert, Quantification of short and medium range order in mixed network former glasses of the system GeO_2-$NaPO_3$: A combined NMR and X-ray photoelectron spectroscopy study, J. Phys. Chem. C **116**, 12747 - 12763 (2012).
21. R.K. Brow, Review: the structure of simple phosphate glasses, J. Non-Cryst. Solids **263&264**, 1-28 (2000).
22. B. J. Berne and R. Pecora, *Dynamic Light Scattering* (John Wiley & Sons, New York, 1976).
23. C. C. Lai, P. B. Macedo, and C. J. Montrose, Light-scattering measurements of structural relaxation in glass by digital correlation spectroscopy, J. Am. Ceram. Soc. **58**, 120 - 123 (1975).

24. P. B. Macedo and A. Napolitano, Inadequacies of viscosity theories for B2O3, J. Chem. Phys. **49**(4) 1887 - 1895 (1968).
25. J. E. Martin and J. P. Wilcoxon, Critical dynamics of the sol-gel transition, Phys. Rev. Lett. **61**(3), 373-376 (1988).
26. M. Adam, M. Delsanti and J. P. Munch, Dynamical studies of polymeric cluster solutions obtained near the gelation threshold: Glasslike behavior, Phys. Rev. Lett. **61**(6), 706-709 (1988).
27. S. Z. Ren, W. F. Shi, W. B. Zhang, and C. M. Sorensen, Anomalous diffusion in aqueous solutions of gelatin, Phys. Rev. A, **45**(4), 2416 (1992).
28. R. Boehmer and C. A. Angell, Correlations of the nonexponentiality and state dependence of mechanical relaxations with bond connectivity in Ge-As-Se supercooled liquids, Phys. Rev. B **45**, 10091 (1992).
29. M. Tatsumisago, B.L. Halfpap, J.L. Green, S.M. Lindsay, and C.A. Angell, Fragility of Ge-As-Se glass-forming liquids in relation to rigidity percolation and the Kauzmann paradox, Phys. Rev. Lett. **64**, 1549-1552 (1990).
30. D.L. Sidebottom and S.E. Schnell, Role of intermediate-range order in predicting the fragility of network-forming liquids near the rigidity transition, Phys. Rev. B **87**, 054202 (2013).
31. D. L. Sidebottom, T. D. Tran, and S. E. Schnell, Building up a weaker network: The effect of intermediate range glass structure on liquid fragility, J. Non-Cryst. Solids **402**, 16 (2014).
32. G. S. Henderson, The germanate anomaly: What do we know? J. Non-Cryst. Sol. **353**: 1695-1704 (2007).

Table 1 Parameters determined from light scattering analysis of $(GeO_2)_x(NaPO_3)_{100-x}$ glass melts.

x (mol% GeO_2)	T_g (±10 C)	β_S	β_F	m (± 5%)	$\langle n \rangle$	ϕ
0	288.0	-	0.43 (±0.05)	80.0	2.00	2.00
5	314.3	0.84 (±0.04)	0.37 (±0.02)	56.1	2.10	2.10
10	367.2	0.78 (±0.05)	0.44 (±0.03)	50.6	2.19	2.14
15	395.7	0.71 (±0.05)	0.41 (±0.02)	43.7	2.31	2.20
20	458.0	0.64 (±0.05)	0.41 (±0.07)	48.0	2.39	2.19
25	441.0 (±15 C)	0.59 (±0.06)	0.46 (±0.06)	54.5	2.49	2.13
30	479.4	0.58 (±0.08)	0.44 (±0.06)	59.7	2.58	2.12
35	482.7	0.56 (±0.04)	0.45 (±0.03)	56.3	2.69	2.13
40	487.3	0.58 (±0.11)	0.48 (±0.05)	60.0	2.79	2.15

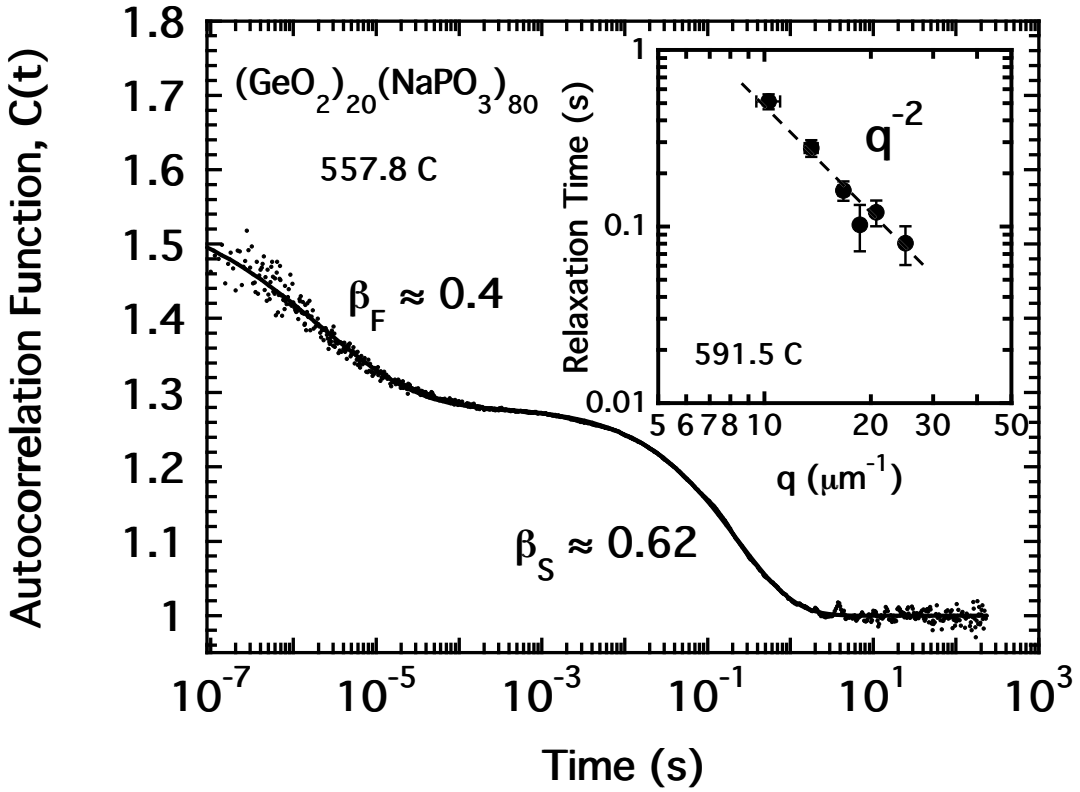

Fig. 1 Autocorrelation function obtained in $(GeO_2)_{20}(NaPO_3)_{80}$ glass melt at 557.8 C displaying two non-exponential relaxations discussed in the text. Solid line is a fit to a pair of stretched exponentials (see Eq. 4 and 5). Inset shows the scattering wavevector dependence for the relaxation time of the slower relaxation process measured in the same melt at 591.5 C.

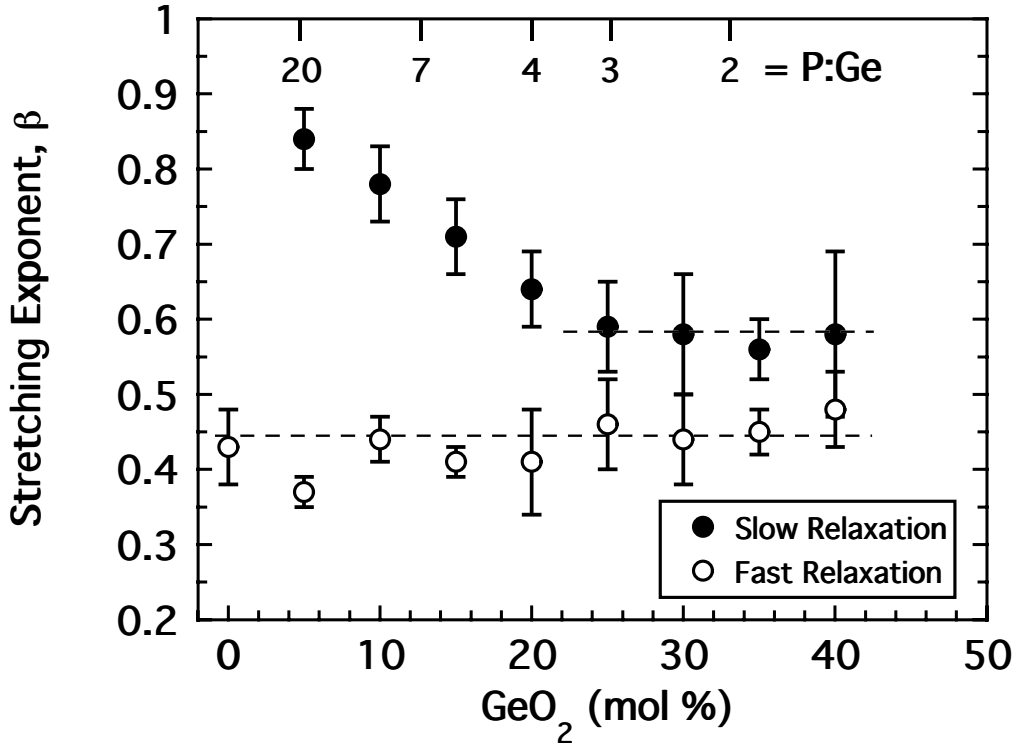

Fig. 2 Variation of the stretching exponents for both the fast α-relaxation and the slow diffusive relaxation as a function of added GeO_2. Ratio of phosphorus to germanium is indicated at the top of the figure.

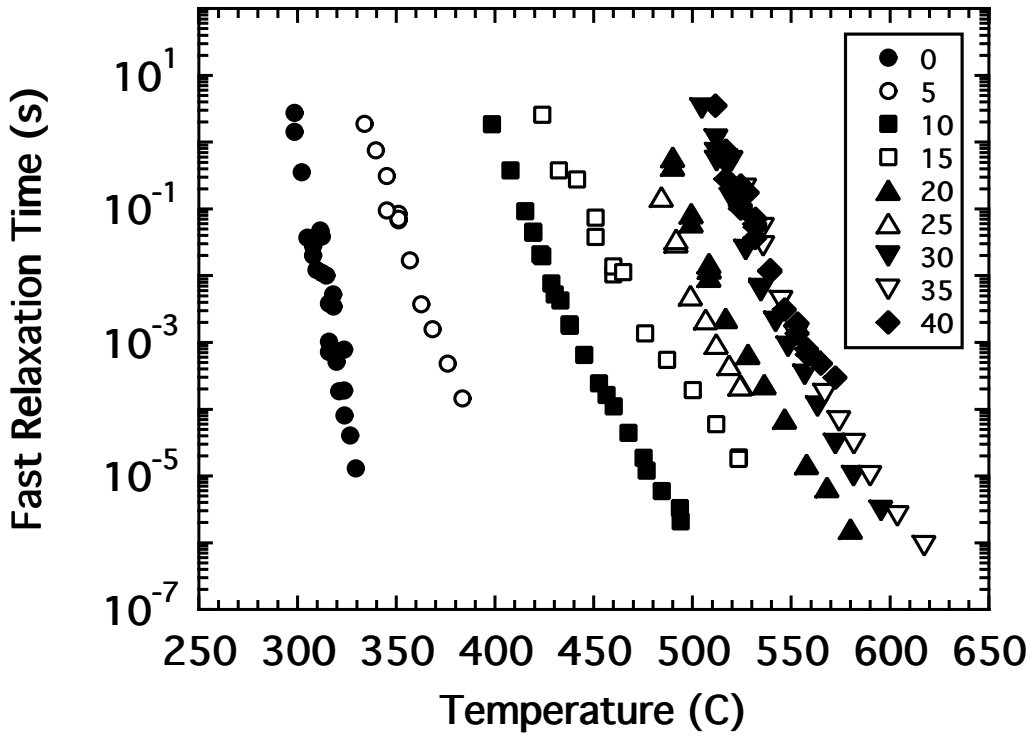

Fig. 3 Temperature dependence of the fast α-relaxation with mol% GeO_2 indicated in the key.

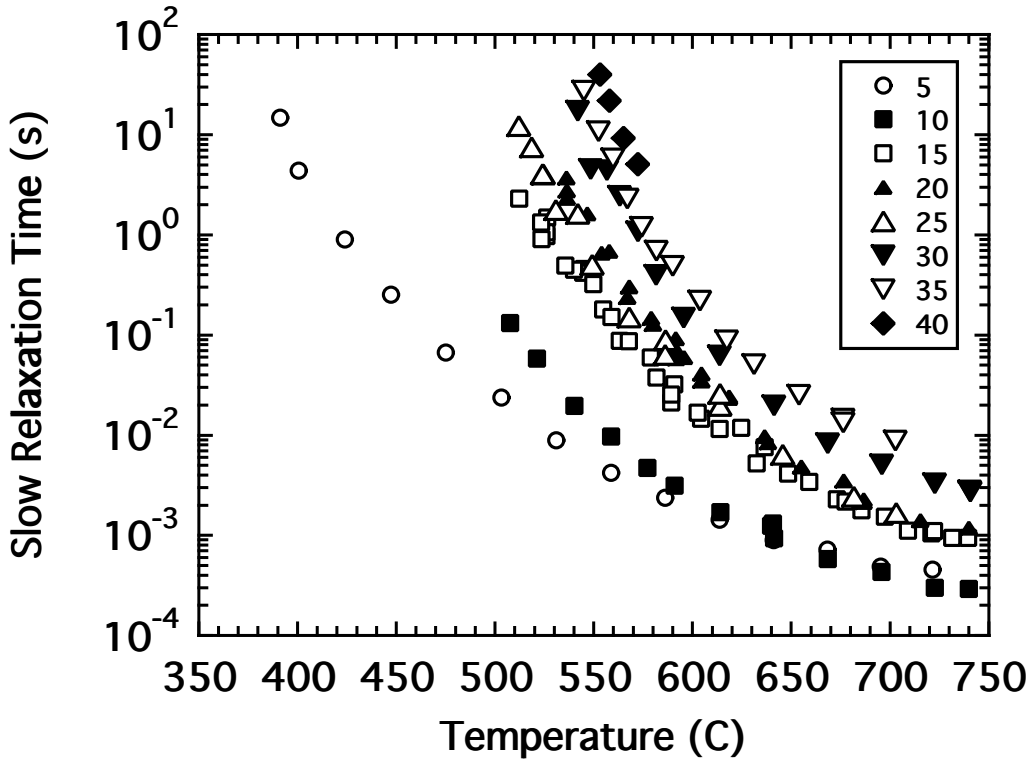

Fig. 4 Temperature dependence of the slow diffusive relaxation with mol% GeO_2 indicated in the key.

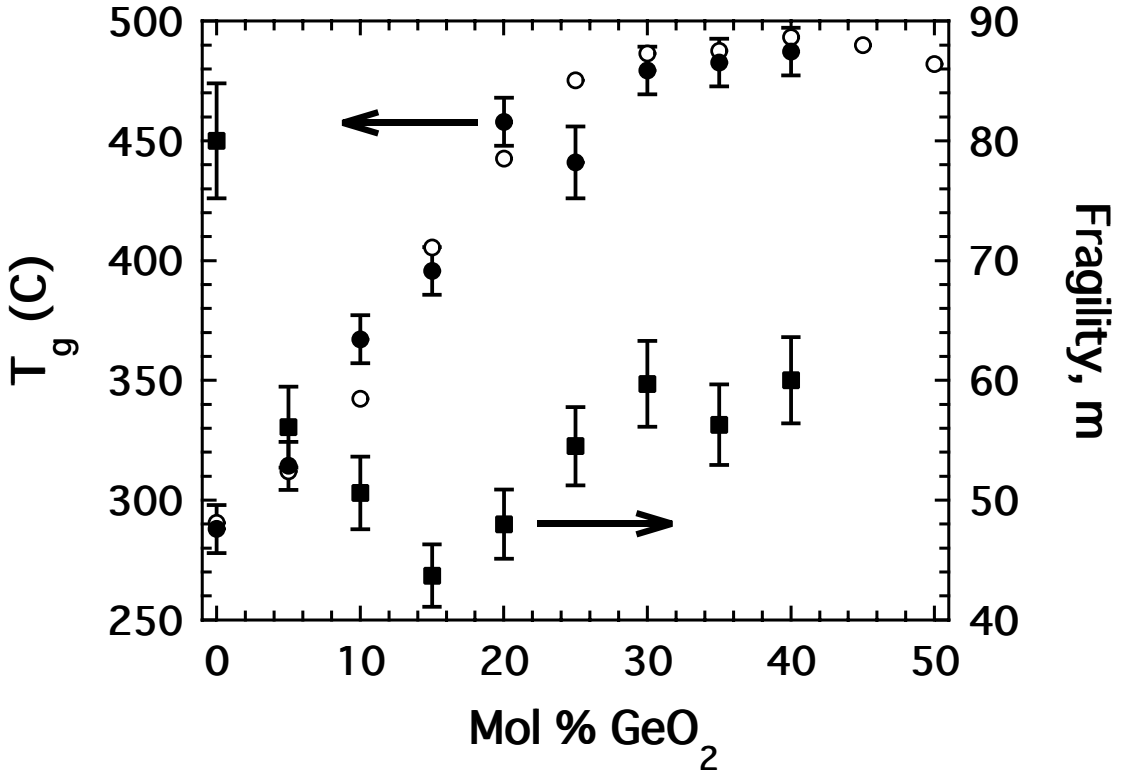

Fig. 5 Variation of the glass transition temperature (solid circles) determined in the present study and those (open circles) reported in the literature [20] as a function of added GeO_2 along with values of fragility index (solid squares).

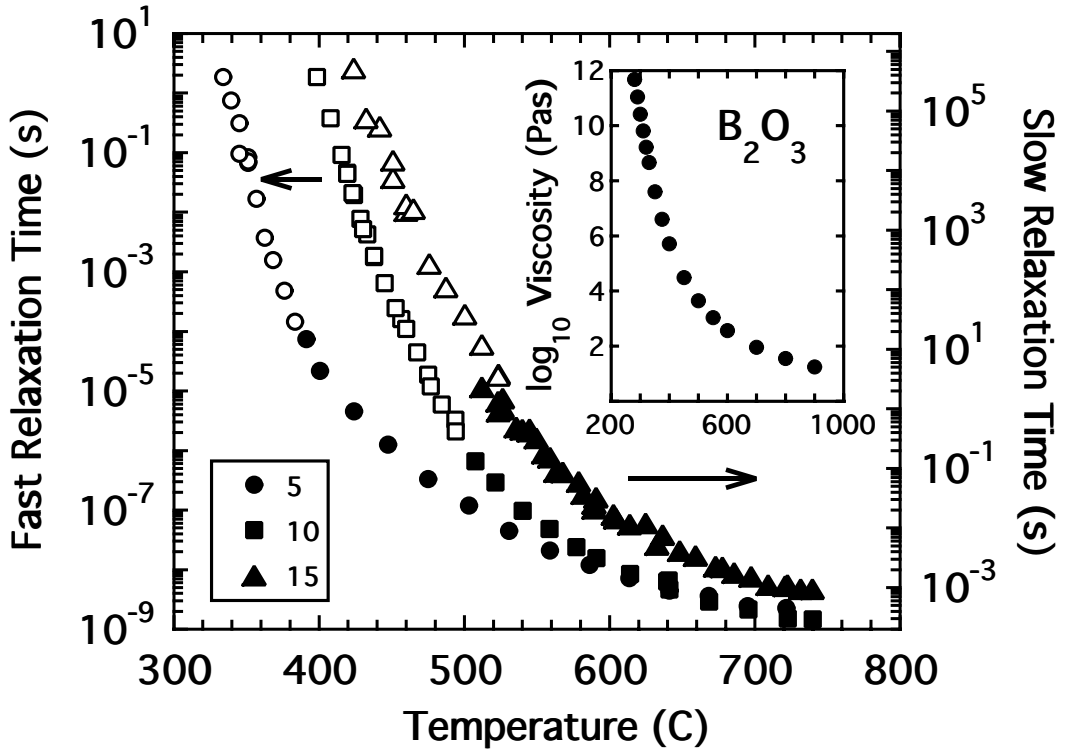

Fig. 6 Fast (open symbols) and slow (solid symbols) relaxation times plotted together with shift by 2 x 10^5 to illustrate the alignment of the two processes for low levels of GeO_2 (mol% provided in key). Inset shows the viscosity of B_2O_3 [24] to illustrate the similarity with the aligned relaxation times.

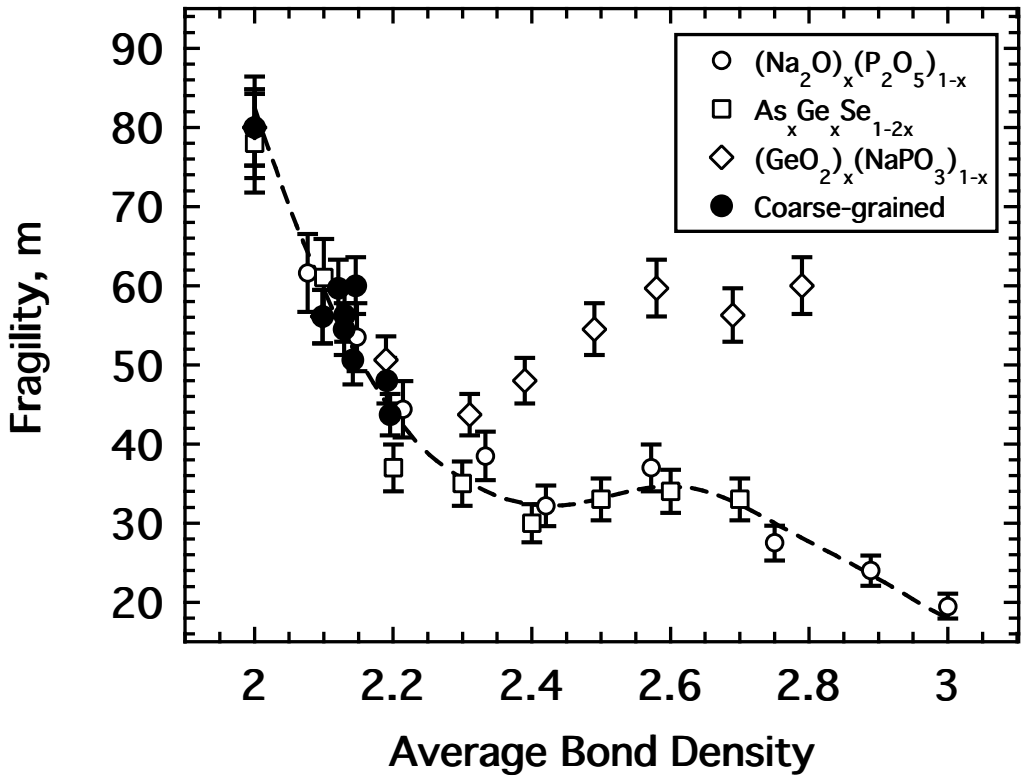

Fig. 7 The fragility index of sodium phosphate melts [14] (open circles, plotted against $\langle n \rangle$), chalcogenides [28] (open squares, plotted against $\langle r \rangle$) and the present glass melts plotted both against $\langle n \rangle$ (open diamonds) and against the coarse-grained connectivity ϕ (solid circles). Dashed line indicates a mastercurve formed by the sodium phosphate and chalcogenide data sets.

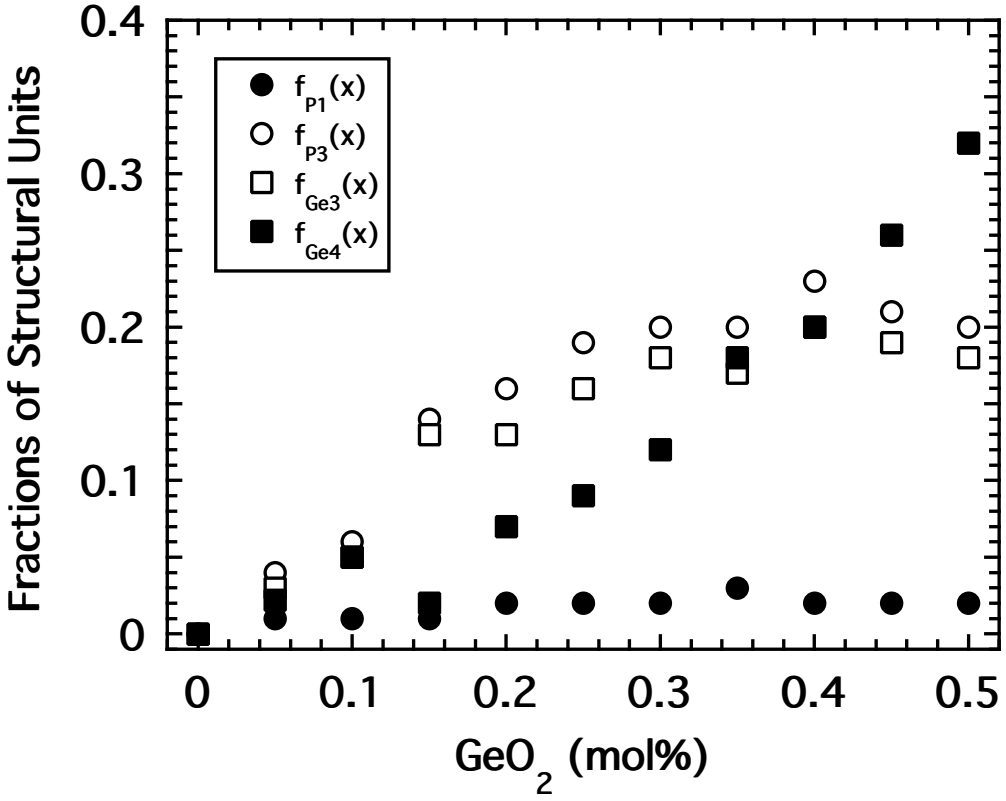

Fig. 8 The fractions of structural units, $f_{P1}(x)$, $f_{P3}(x)$, $f_{Ge3}(x)$ and $f_{Ge4}(x)$ reported in the NMR study [20] showing the complex compositional variations. The balance of the units, $f_{P2}(x)$, have been omitted for clarity.

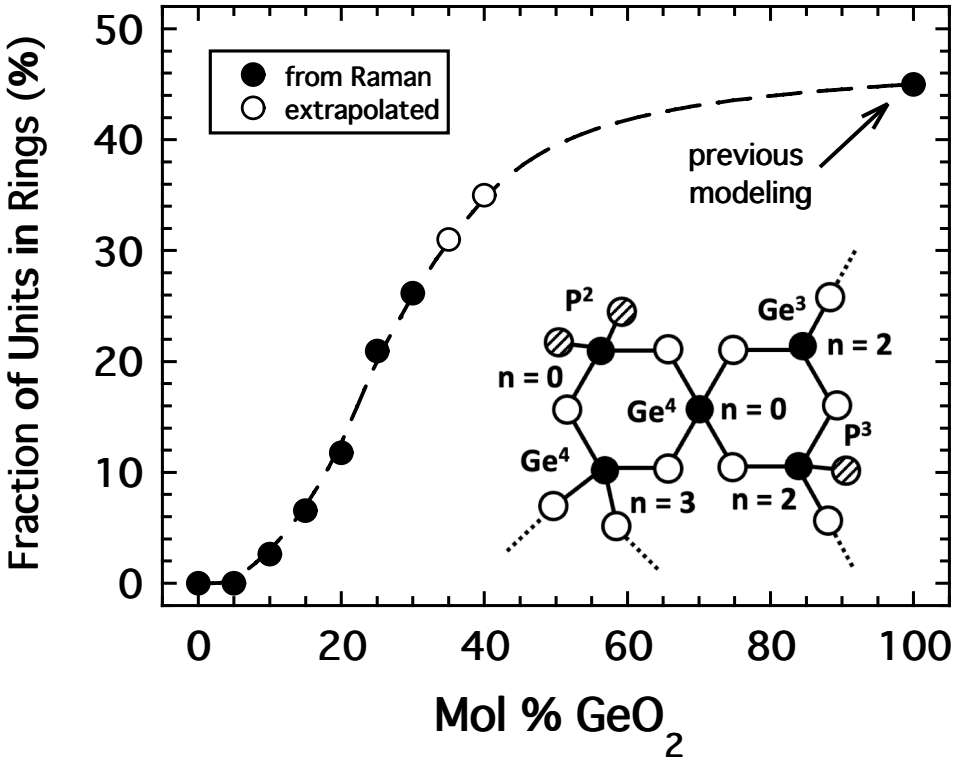

Fig. 9 The fraction of structural units in rings based on analysis of the Raman spectra [20] (solid circles) and from previous coarse-graining [31] in GeO_2. The dashed line is a computer-generated smooth fit to the solid circles and the open circles are ring fractions determined from that fit. Inset is a cartoon illustrating the coarse-graining designations of various structural units (open circle, bridging oxygen; hashed circle, non-bridging oxygen; solid circle, either P or Ge as indicated).